

ANSYS HFSS Compliance with IEEE/IEC 62704-1

A report showing how HFSS complies with the accepted code validation and canonical benchmark problems prescribed in IEC 62704-1

1. HFSS - AN INTRODUCTION

HFSS™ uses a numerical technique called the Finite Element Method (FEM). This is a procedure where a structure is subdivided into many smaller subsections called finite elements. The finite elements used by HFSS are tetrahedral. A solution is found for the fields within the finite elements, and these fields are interrelated so that Maxwell's equations are satisfied across inter-element boundaries, yielding a field solution for the entire, original, structure. Once the field solution has been found, the generalized S-matrix solution is determined.

HFSS's proven track record in a broad range of electromagnetic applications, and its ability to use a tetrahedral mesh that conforms to complicated geometries, employing arbitrarily small elements where needed, and not-very-small elements elsewhere make it a highly accurate and very efficient numerical solution to many electromagnetic problems including the calculation of Specific Absorption Rate (SAR). This document will show that HFSS can be used for the calculation of SAR by demonstrating that the numerical results obtained by HFSS are accurate to within an acceptable level. It will show that HFSS has the accuracy required by applying the code validation methods and reference models described in IEC 62704-1, and demonstrating that HFSS does indeed provide numerical results that are within the accepted tolerances as specified in IEC 62704-1.

While the IEC 62704-1 standard specifically applies to Finite Difference Time Domain (FDTD) methods, the code validation and canonical problems can easily be used for the validation of HFSS as well. While there are mathematical differences between FDTD and FEM the following applies to how the finite element method is implemented within HFSS.

- It is based on differential equations, not on integral equations.
- The size of the computational domain is finite. Radiation towards infinity is implemented through an absorbing boundary condition, a Perfectly Matched Layer, or an implementation of the Boundary Element Method (BEM) on outer boundaries. Radiated fields outside the domain can be computed by integrating over a boundary that encloses the radiating structure.
- After applying excitations and boundary conditions and discretizing the computational domain into a mesh, a matrix equation results in which the matrix is large, sparse, and banded. "Large" is a consequence of having a large number of unknowns, several per mesh element on a large mesh. "Sparse" and "banded" are consequences of the fact that all interactions are formulated as local interactions.
- In the limit of infinitesimally small mesh elements, the solution approaches the exact solution to Maxwell's equations.

Appendix A contains more information on the Finite Element Method, along with references to literature.

2. CODE VALIDATION

2.1 Introduction

This section provides procedures for the following two levels of code validation.

- Code Performance Validation
- Canonical Benchmarks

This section follows the chapter on Code Validation in IEC 62704-1 with modifications proper to the Finite Element Method. Below, the objectives of the different levels of validation are described.

2.2 Code performance validation

The code performance validation provides methods to determine that the finite-element algorithm in HFSS has been implemented correctly and works accurately within the constraints due to the finite numerical accuracy. It further determines the quality of absorbing boundary conditions and certain parts of the post processing algorithms that are part of HFSS. All canonical benchmarks can be compared to analytical solutions of the physical problem or its numerical representation. The methods characterize the implementation of the finite-element algorithm used by HFSS in a very general way. They are defined such that it is not possible to tune the implementation for a particular benchmark or application without improving the overall quality of the code.

2.3 Canonical benchmarks

The canonical benchmarks assess the cumulative accuracy of HFSS and its applicability considering the interaction of its different modules, such as mesh generation, computational kernel, representation of sources, data extraction algorithms of the post processor, etc.

2.4 CODE PERFORMANCE VALIDATION

2.4.1 Propagation homogeneous medium

A straight rectangular waveguide with ports on both ends is well suited as a first test of an implementation of the Finite-Element Method used by HFSS. The waveguide has a width of 20 mm, a height of 10 mm and a length of 300 mm. The waveguide is filled homogeneously with a material which, in three separate simulations, shall assume the following properties:

- $\epsilon_r = 1, \sigma = 0 \text{ S/m}$;
- $\epsilon_r = 2, \sigma = 0 \text{ S/m}$;
- $\text{Re}(\epsilon_r) = 2, \sigma = 0.2 \text{ S/m}$.

To verify that the mesh used by HFSS is independent of orientation, the waveguide has been rotated so that it is not parallel with any principal coordinate plane (XY, XZ, YZ). The waveguide is driven in the TE₁₀ mode at 10 GHz. Reported are the magnitudes of S₂₁ and S₁₁, as well as the values of the real and imaginary parts of the propagation constant γ . Table 1, below provides the reference values [B1], acceptable result criteria, as well as the simulated results.

Re(ϵ_r)	1	2	2
σ	0	0	0.2
S ₂₁ reference value	1	1	8.7×10^{-5}
Criterion for S ₂₁	≥ 0.9999	≥ 0.9999	$\pm 5 \times 10^{-6}$
S ₂₁ simulated results	1	1	8.7×10^{-5}
S ₁₁ reference value	0	0	0
Criterion for S ₁₁	≤ 0.003	≤ 0.003	≤ 0.003
S ₁₁ simulated results	0	0	0
Re(γ) reference value	0	0	31.17 m ⁻¹
Criterion for Re(γ)	± 0.1 m ⁻¹	± 0.1 m ⁻¹	$\pm 2\%$
Re(γ) simulated results	0	0	31.17
Im(γ) reference value	138.75 m ⁻¹	251.35 m ⁻¹	253.28 m ⁻¹
Criterion for Im(γ)	$\pm 2\%$	$\pm 2\%$	$\pm 2\%$
Im(γ) simulated results	138.75	251.35	253.28

Table 1 - Criteria for the waveguide evaluation

As is seen in the above table, HFSS meets the criteria for properly and accurately calculating the waveguide problem.

2.4.2 Planar dielectric boundary

In order to test the reflection of a plane wave by a dielectric boundary, a rectangular waveguide can again be used. It is well known that the TE₁₀ mode can be thought of as a superposition of two plane waves [B1]. Each wave's direction of propagation makes an angle θ with the axis of the wave guide, given by

$$\cos^2\theta = 1 - (c/2af)^2 \quad (1)$$

where c is the speed of light, a is the width of the wave guide and f is the frequency.

Assuming the axis of the waveguide is the Z axis and assuming the waveguide is filled with vacuum for $Z > 0$ and filled with dielectric 1 with complex relative permittivity ϵ_r for $Z < 0$, Fresnel reflection coefficients for the TE and the TM cases, defined as ratios of electric field strengths, are given by [B2]

$$R^{TE} = (k_{0,z} - k_{1,z}) / (k_{0,z} + k_{1,z}) \quad (2)$$

$$R^{TM} = (\epsilon_r k_{0,z} - k_{1,z}) / (\epsilon_r k_{0,z} + k_{1,z}) \quad (3)$$

where $k_{0,z}$ and $k_{1,z}$ denote the z component of the propagation vector of the plane wave in vacuum and in the dielectric, respectively. They can be evaluated through

$$k_{0,z} = k_0 \cos\theta \quad (4)$$

$$k_{1,z} = k_0 \sqrt{(\epsilon_r - \sin^2\theta)} \quad (5)$$

Finally, ϵ_r is complex and is given by

$$\epsilon_r = \text{Re}(\epsilon_r) - j\sigma/(2\pi f\epsilon_0) \quad (6)$$

where $\text{Re}(\epsilon_r)$ denotes the real part of the relative permittivity and σ is the conductivity of the medium.

For this test, a 20 mm × 10 mm waveguide with a length of 60 mm, as shown in Figure 1, was created. The top half was filled with vacuum and the bottom half with dielectric.

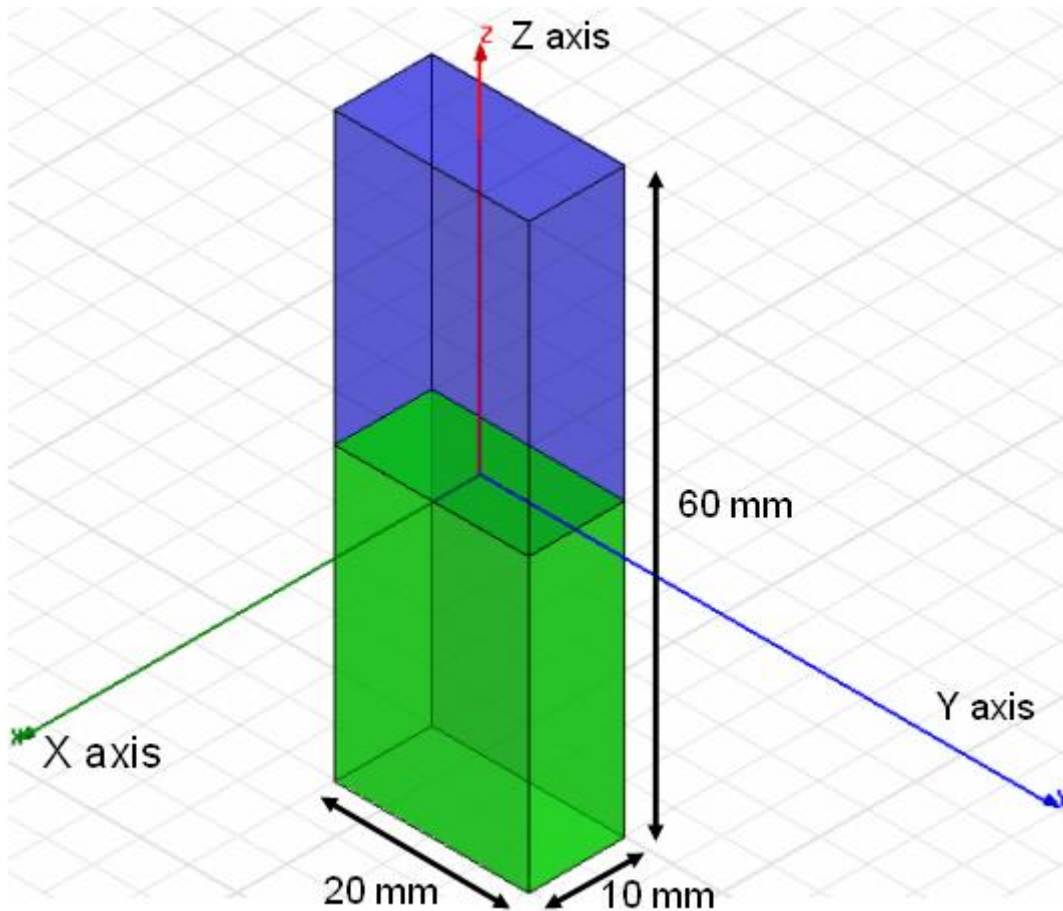


Figure 1 - Waveguide filled half vacuum and half dielectric

In one copy of the model, all side walls were lossless metal, such that the dominant mode is the TE_{10} mode with propagation constant 138.75 m^{-1} at 10 GHz and represents the TE case in the reflection analysis. In the other copy of the model, the side walls that are parallel to the YZ plane were perfect magnetic conductors while the other walls were perfect electric conductors, such that the second mode (after a TEM mode which won't be used in this test) has propagation constant 138.75 m^{-1} at 10 GHz and represents the TM case in the reflection analysis.

Before simulation, the waveguides were rotated over an arbitrary angle such that no face is parallel with any coordinate plane. The waveguides were driven at 10 GHz in the proper mode. In doing so, it is good practice to calculate all propagating modes, but the coupling between modes is expected to be negligible. Simulations were run for the cases of lossless and lossy dielectric as shown in Table 2. For the HFSS to pass the test, according to IEC 62704-1, the results need to be within 2% of the analytical values given in Table 2.

$\text{Re}(\epsilon_r)$	σ (S/m)	R^{TE}	$R^{\text{TE}} - \text{Simulated}$	R^{TM}	$R^{\text{TM}} - \text{Simulated}$
4	0	0.4739	0.4739	0.1763	0.1763
4	0.2	0.4755	0.4755	0.1779	0.1779
4	1	0.5105	0.5105	0.2121	0.2121

Table 2 - Reflection at a dielectric interface

As can be seen in Table 2, HFSS produces results that are identical to the analytical results.

2.4.3 Absorbing boundary conditions

The performance of an absorbing boundary condition (ABC) can be assessed analogously to the procedure used for the assessment of the numerical reflection. The computational domain shall be filled homogeneously with vacuum ($\epsilon_r=1$, $\sigma = 0$) and truncated with an ABC at a position of $z = 120$ mm in front of the excitation. For this example the TE₀₁ moded waveguide is truncated with a perfectly match layer (PML) object. The figure below shows the results for the reflection coefficient from HFSS where the waveguide geometry is aligned along the three principle axis of the global coordinate system and oriented at 45 degrees away from the Z axis in the ZX plane of the global coordinate system. The solid red line is for Orientation along the Z axis, dotted blue line is for orientation along the Y axis, dashed green line is for orientation along the X axis and dotted-dashed black line is for orientation at 45 degrees tilted away from the z-axis rotated about X. Overlaid in this plot is a limit line composed of vertically oriented grey lines that designate the upper margins for acceptable reflection from the truncation boundary. It can be seen that HFSS satisfies this condition at all frequencies and all rotation angles for the waveguide. For this simulation the structure is solved with a conformal and automatically adaptively refined finite element tetrahedral mesh at 2 GHz with a frequency sweep from 500 MHz to 3 GHz.

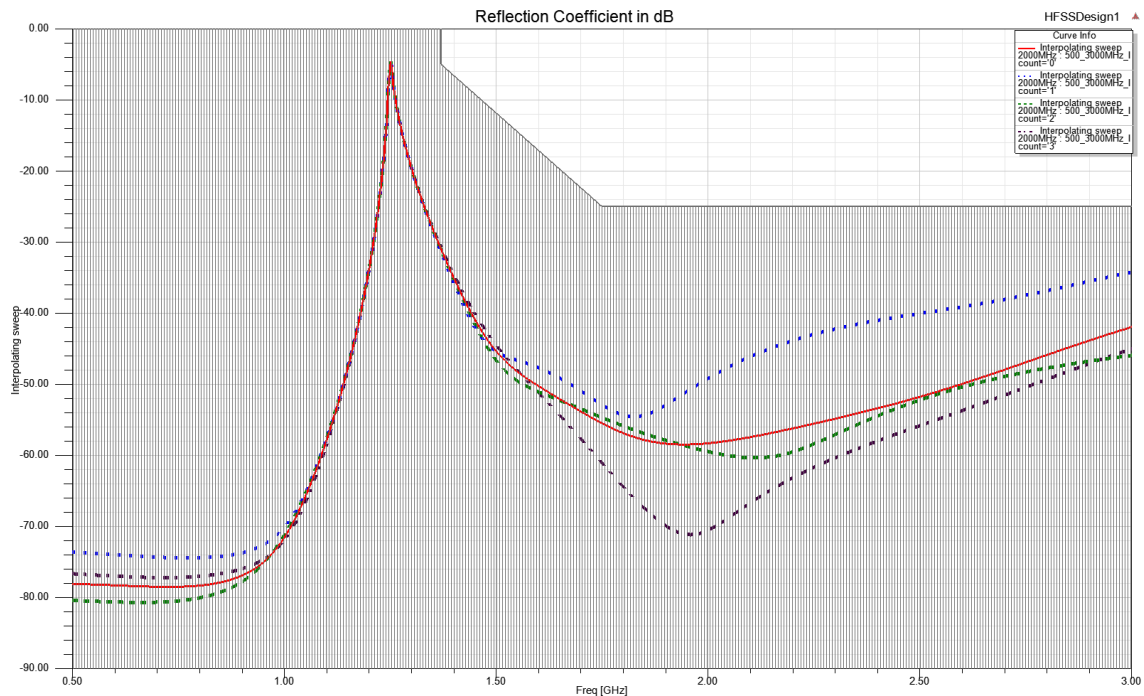


Figure 2 - Reflection coefficient for waveguide at various orientations truncated in a PML

2.5 CANONICAL BENCHMARKS

2.5.1 Generic dipole antenna

The feed-point impedance and the far-field pattern of a dipole antenna (half-wavelength dipole at 1 GHz) were evaluated at 1 GHz. The dipole had a length of 150 mm and a diameter of 4 mm. The feeding gap size was 2 mm. The computational domain extended at least 200 mm from the dipole in all directions.

The quantities for evaluation, simulated results and the maximum permitted error are given in Table 3. The power budget is defined as the difference between the radiated power as determined by the far-field evaluation and the accepted power as determined from S_{11} . Reference results were computed using the Method of Moments.

Quantity	Simulated Results	Limit
$\text{Re}\{Z\}$ at 1.0 GHz	105.2	$40 \Omega < \text{Re}\{Z\} < 140 \Omega$
$\text{Im}\{Z\}$ at 1.0 GHz	42.2	$30 \Omega < \text{Im}\{Z\} < 130 \Omega$
Frequency for $\text{Im}\{Z\} = 0$	918 MHz	$850 \text{ MHz} < f < 950 \text{ MHz}$
Power budget 1.0 GHz	1.03	5%

Table 3 - Results of the dipole evaluation

2.5.2 Microstrip terminated with Absorbing Boundary Condition

The propagation constant and wave impedance of a microstrip line and the reflection coefficient for quasi-TEM operation were evaluated.

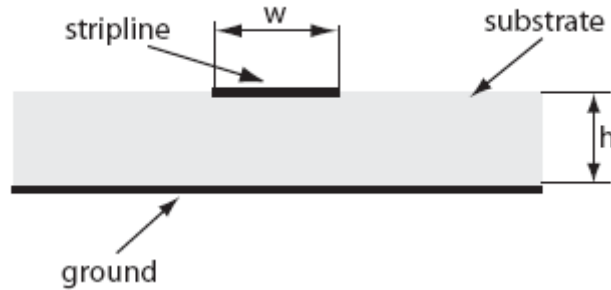


Figure 3 - Geometry in cross section of the micro strip line

The substrate was lossless and had a relative permittivity of 3.4. The geometry of the micro strip line is given in Figure 2. The line was terminated with an absorbing boundary condition. For an impedance close to 50Ω , the width w of the micro strip and the height h of the substrate shall be 2.8 mm and 1.2 mm, respectively. The thickness of the stripline is negligible with respect to the other dimensions of the geometry. It can therefore be modeled as an infinitely thin sheet.

The propagation constant, the characteristic impedance and the reflection coefficient $|S_{11}|$ is reported over the entire frequency range 0.5 GHz to 2.0 GHz, in table 4.

Quantity	Reference	Simulated Results	Limit
Re{Z}	50 Ω	48.3 Ω <Re{Z}<50.8 Ω	45 Ω < Re{Z} < 55 Ω
Im{Z}	0	-1.2 Ω < im{Z} < 1.2 Ω	-2 Ω < Im{Z} < 2 Ω
Reflection Coefficient	- ∞	~ -37.4 dB	<-20dB

Table 4 - Results of the micro-strip evaluation

Table 4 clearly shows that the results from HFSS are well within the numerical accuracy that is required.

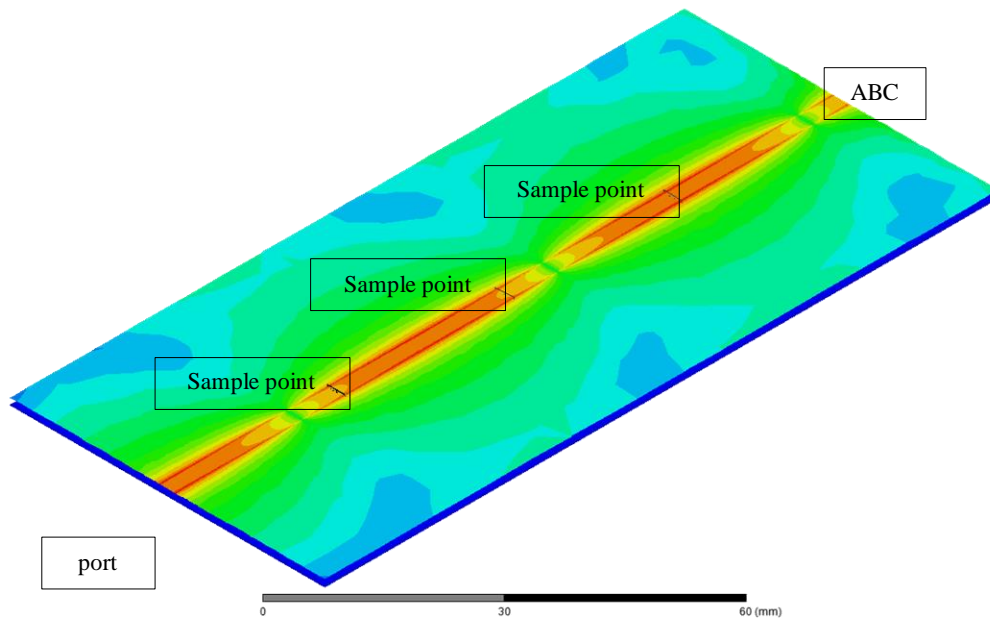


Figure 4 - E-field distribution on substrate surface at phase=0 deg

In HFSS current in trace and voltage difference between trace (length=120mm) and groundplane is computed at three points along the microstrip separated by 30mm. Z at points along line is computed as voltage/current. Current is computed through an integration of the H-field about a loop around the trace and voltage computed by integrating E field along line from bottom of trace to groundplane.

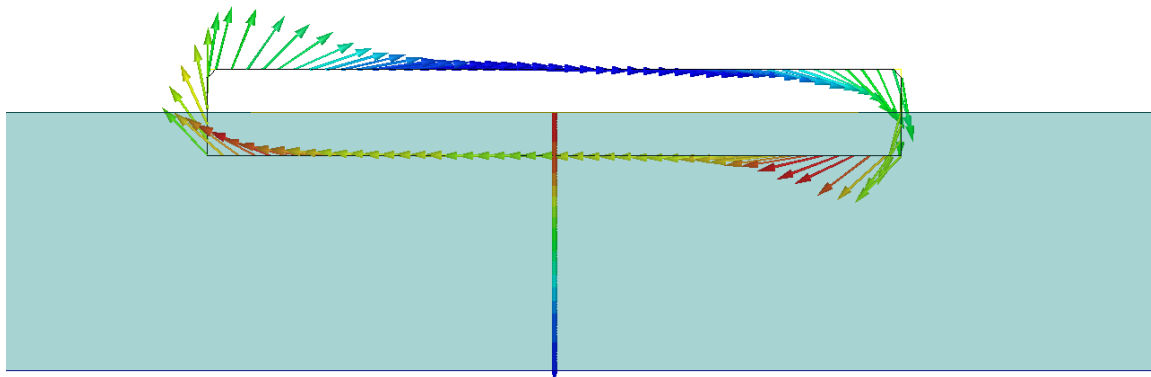


Figure 5 - Cross section view showing current loop and voltage line

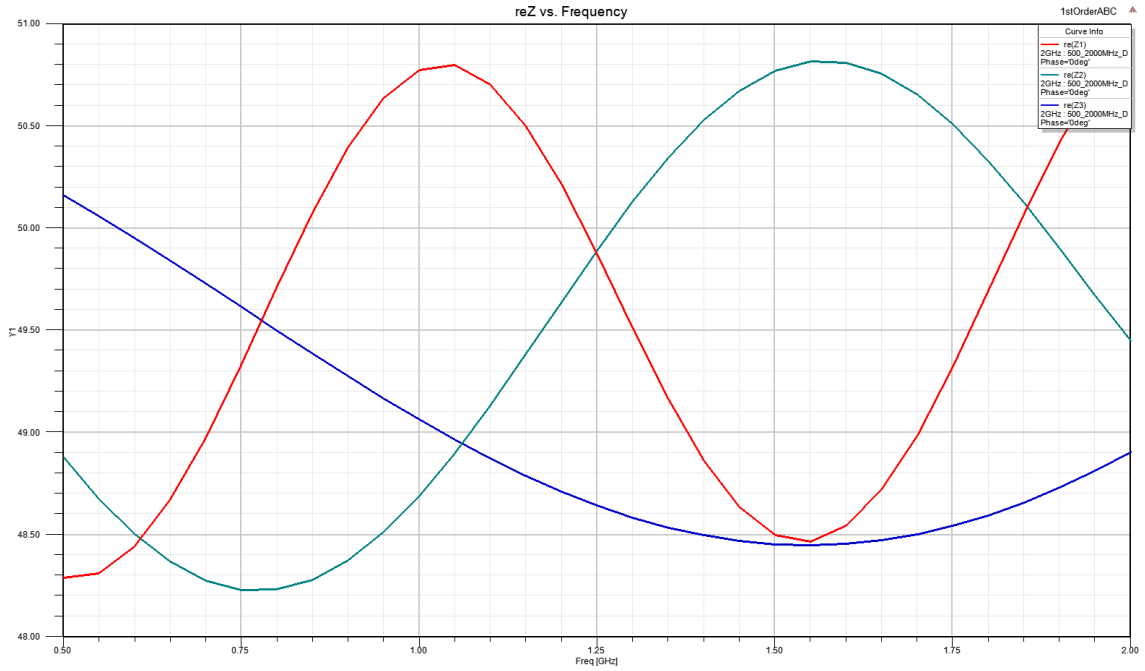


Figure 6 - Plot of reZ at sample points as function of frequency

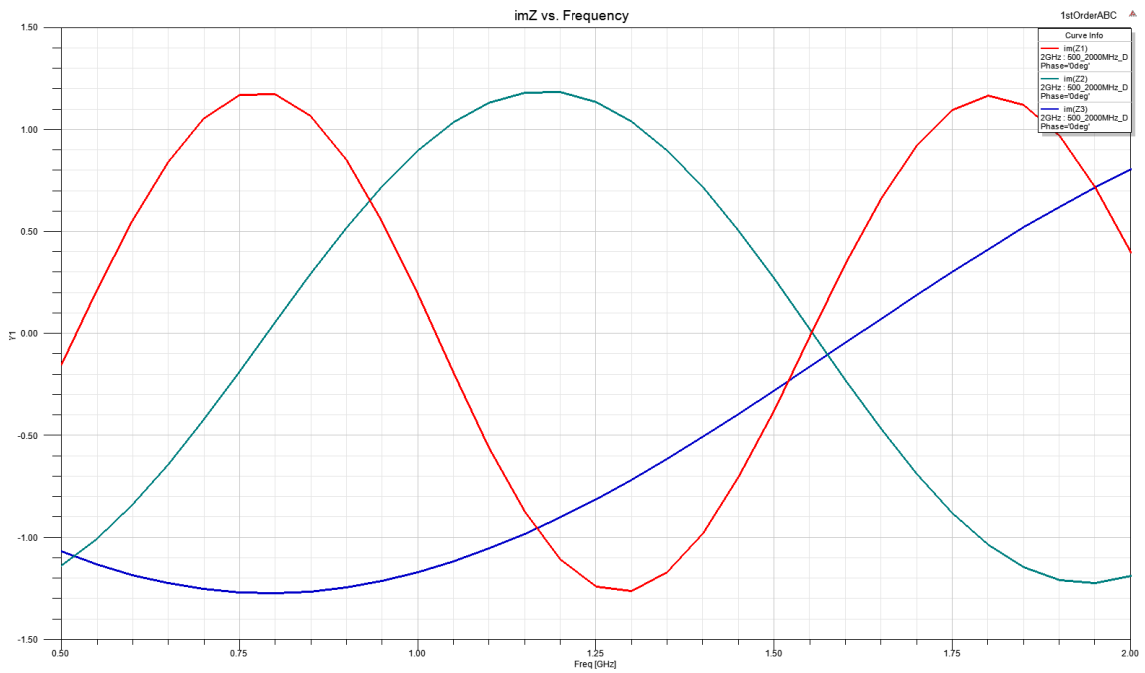


Figure 7 - Plot of imZ at sample points as function of frequency

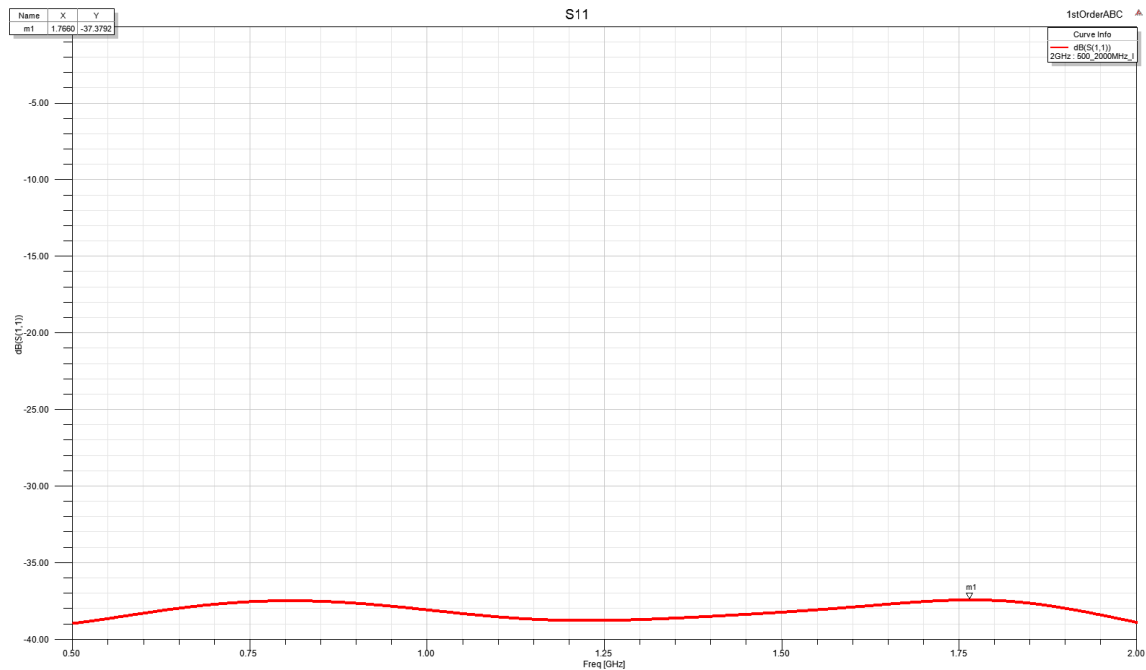


Figure 8 - S11 vs. Frequency for Microstrip

2.5.3 SAR Calculation SAM Phantom – Generic Phone

The benchmark described in Beard et al. [B15] shall be repeated for the SAM phantom with the generic phone in the “touch” and the “tilted” position IEEE 1528 [B16]) at 835 MHz and 1900 MHz. One gram (1g) and 10g peak spatial-average SAR values shall be reported for the two positions and frequencies. The SAR results shall be normalized to the feed-point power. They must be within the two times the standard deviation reported by Beard et al. [B15]. The center points of the cubical averaging volumes of the 1g and 10g peak spatial-average SAR shall not deviate by more than half a side length of the averaging cube (5mm for the 1g cube and 10.8mm for the 10g cube). Supplemental information on the configuration can be found in (Kainz et al. [B17]).

For the HFSS results Tables 1 and 2 below summarize the results for the 1g and 10g equivalent volume respectively for the cheek and tilt position at 835 and 1900 MHz. The column labeled ‘IEEE 1528.1’ computes the SAR through the voxelized approach outlined in section 3.2 of [B18].

Frequency and Position	Simulation Results IEEE 1528.1	Reference
835 MHz Cheek	7.70	7.47 (0.4)
835 MHz Tilt	5.23	4.93 (0.64)
1900 MHz Cheek	6.91	8.28 (1.58)
1900 MHz Tilt	9.48	11.97 (3.10)

Table 5 - Results 1g SAR Analysis.

Frequency and Position	Simulation Results IEEE 1528.1	Reference (Beard et. al.)
835 MHz Cheek	5.41	5.26 (0.27)
835 MHz Tilt	3.63	3.39 (0.26)
1900 MHz Cheek	4.47	4.79 (0.73)
1900 MHz Tilt	5.65	6.78 (1.37)

Table 6 - Results 10g SAR Analysis.

Figure 9 below shows an image of the SAM phantom positioned with respect to the generic phone model. The phone is oriented along the Y axis of the global coordinate system which with the SAR voxelization is constructed for the SAR calculation. Overlaid on the model of the phantom is a 2D surface plot of the localized SAR, the point by point SAR not integrated over a volume average, for a 1W amplitude excitation at the phone antenna port. Figure 10 shows the configuration of the head phantom and generic mobile phone at the 15 degree tilt angle away from the cheek.

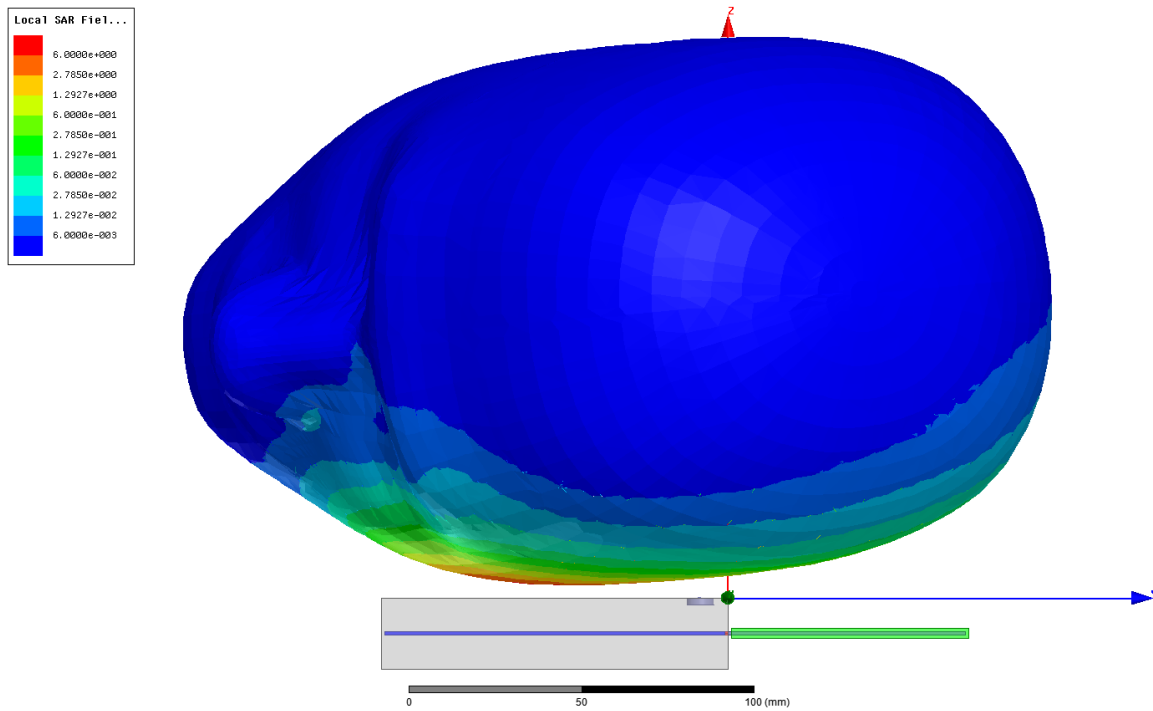


Figure 9 - Cheek position with local SAR plot on head phantom for 835MHz (1W)

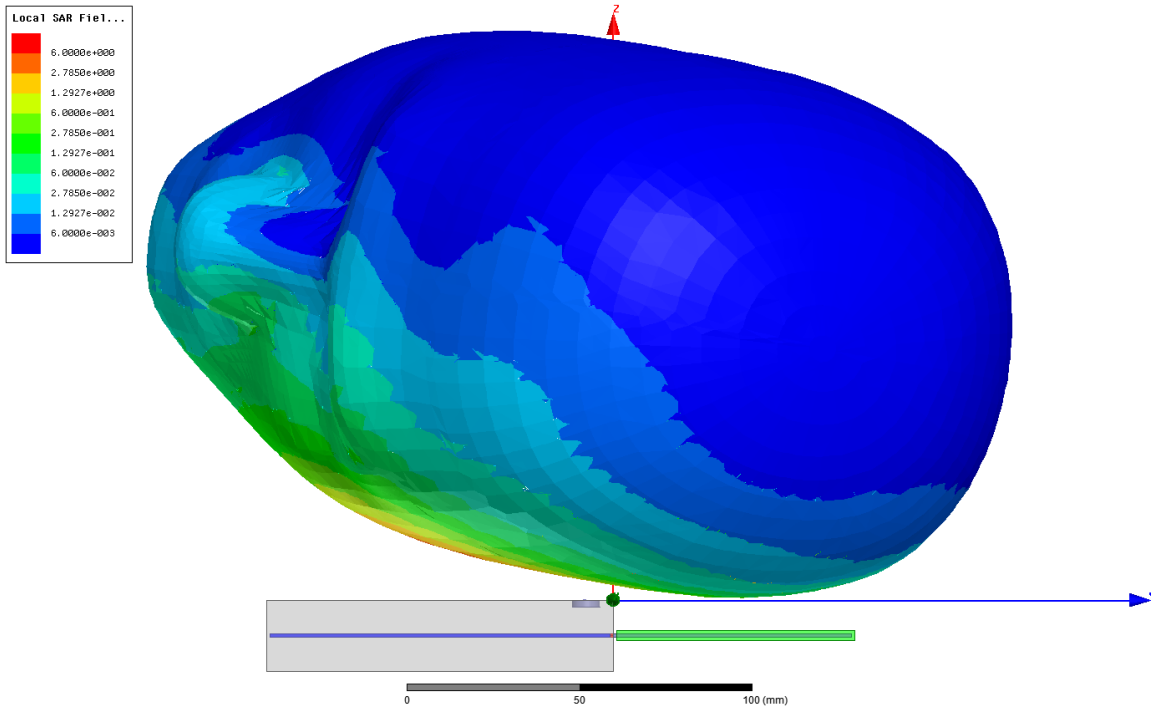


Figure 10 - Tilt position with local SAR plot on interior head phantom for 835MHz (1W)

2.5.4 Setup for system performance check

To further validate the accuracy of HFSS wrt SAR analysis simulation were run to mimic the measurement system performance check as outlined in [B16]. The summary for the simulation results for HFSS as compared to results for FDTD are outlined in table 7 below.

Freq. (MHz)	1g SAR FDTD	1g SAR HFSS '14	10g SAR FDTD	10g SAR HFSS '14	L SAR fp FDTD	L SAR fp HFSS '14	L SAR 2cm FDTD	L SAR 2cm HFSS '14
300	3.02	3.09	2.04	2.07	4.40	4.59	2.10	2.14
450	4.92	4.68	3.28	3.29	7.20	7.63	3.20	3.27
835	9.56	9.57	6.22	6.23	14.1	14.79	4.90	4.89
900	10.9	10.88	6.99	6.96	16.4	17.09	5.40	5.42
1450	29.0	29.13	16.0	16.03	50.2	53.73	6.50	6.28
1800	38.4	39.32	20.1	20.47	69.5	75.57	6.80	6.63
1900	39.7	39.94	20.5	20.30	72.1	77.10	6.60	6.35
2450	52.4	55.09	24.0	24.86	104	117.31	7.70	7.65
3000	63.4	63.68	25.6	25.28	142	155.34	9.50	9.71

Table 7 - ANSYS HFSS Results: Compared to FDTD simulations from Page 93 of standard

For the sake of comparison the same data is analyzed in terms of percent difference between results from HFSS and FDTD in table 8 below. In general there is very good agreement between the two methodologies.

Freq. (MHZ)	% diff 1g average	% diff 10g average	% diff Feed Point	% diff 2cm offset
300	2.3%	1.5%	4.3%	1.9%
450	4.9%	0.3%	6.0%	2.2%
835	0.1%	0.2%	4.9%	0.2%
900	0.2%	0.4%	4.2%	0.4%
1450	0.4%	0.2%	7.0%	3.4%
1800	2.4%	1.8%	8.7%	2.5%
1900	0.6%	1.0%	6.9%	3.8%
2450	5.1%	3.6%	12.8%	0.6%
3000	0.4%	1.3%	9.4%	2.2%

Table 8 – Percent difference between FDTD and HFSS simulation of flat phantom

REFERENCES

- [B1] Rizzi, P.A., "Microwave Engineering – Passive Circuits," Prentice Hall, Inc., 1988.
- [B2] Chew, W.C., "Waves and Fields in Inhomogeneous Media," IEEE Press, 1995, Chapter 2.
- [B3] P.P. Silvester and R.L Ferrari, "Finite Elements for Electrical Engineers", Cambridge University Press, second edition 1990, ISBN 0 521 37829 X (paperback) 0 521 37219 4 (hardcover)
- [B4] Jianming Jin, "The Finite Element Method in Electromagnetics", John Wiley and Sons, Inc., 1993, ISBN 0-471-58627-7
- [B5] Z.J. Cendes and J. Lee, "The Transfinite Element Method for Modeling MMIC Devices", IEEE Transactions on Microwave Theory and Techniques, Vol. 36, No. 12, pp. 1639-1649, December 1988
- [B6] J.E. Bracken, D.K. Sun and Z.J. Cendes, "S-Domain Methods for Simultaneous Time and Frequency Characterization of Electromagnetic Devices", IEEE Trans. MTT, Vol. 46, No. 9, pp. 1277-1290, September 1998.
- [B7] D.-K. Sun, Z.J. Cendes, J.-F. Lee, "ALPS - A new fast frequency-sweep procedure for microwave devices", IEEE Trans. MTT, Vol. 49, No. 2, pp. 398 – 402, Feb. 2001.
- [B8] O. Ramahi and R. Mittra, "Finite-element analysis of dielectric scatterers using the absorbing boundary condition", IEEE Trans. Magnetics, Vol. 25, no. 4, pp. 3043-3045, July 1989.
- [B9] J.P. Berenger, "A Perfectly Matched Layer for the Absorption of Electromagnetic Waves", Journal of Computational Physics, No. 114, pp. 185-200, 1994.
- [B10] J-Y Wu, D.M. Kingsland, J-F Lee and R. Lee, "A Comparison of Anisotropic PML to Berenger's PML and Its Application to the Finite-Element Method for EM Scattering", IEEE Trans. Ant. Propagat., Vol. 45, no. 1, pp. 40-50, 1995.
- [B11] N. Appannagari, I. Bardi, R. Edlinger, J. Manges, M.H. Vogel, Z. Cendes, J. Hadden, "Modeling phased array antennas in Ansoft HFSS", Proceedings of the 2000 IEEE International Conference on Phased Array Systems and Technology, 21-25 May 2000, pp. 323-326.

- [B12] P.P. Silvester and G. Pelosi, "Finite Elements for Wave Electromagnetics", pp. 177-194, IEEE Press, 1994, ISBN 0-7803-1040-3
- [B13] X. Yuan, D.R. Lynch, J. W. Strohbehn, "Coupling of Finite Element and Moment Methods for Electromagnetic Scattering from Inhomogeneous Objects", IEEE Trans. Antennas Propagat., Vol. 38, no. 3, pp. 386-393, 1990.
- [B14] IEEE Std C95.3-2002, "IEEE Recommended Practice for Measurements and Computations of Radio Frequency Electromagnetic Fields With Respect to Human Exposure to Such Fields, 100 kHz-300 GHz"
- [B15] Beard, et. al. "Comparisons of computed mobile phone induced SAR in the SAM phantom to that in anatomically correct models of the human head"
- [B16] IEEE Std 1528TM-2013, "IEEE Recommended Practice for Determining the Peak Spatial-Average Specific Absorption Rate (SAR) in the Human Head from Wireless Communication Devices: Measurement Technique"
- [B17] Kainz, et. al. "Dosimetric Comparison of the Specific Anthropomorphic Mannequin (SAM) to Anatomical Head Models Using a Novel Definition for the Mobile Phone Positioning"
- [B18] IEEE 1528.1 "Draft Recommended Practice for Determining the Peak Spatial-Average Specific Absorption Rate (SAR) in the Human Body from Wireless Communication Devices, 30 MHz – 6 GHz: General Requirements for Using the Finite Difference Time Domain Method for SAR Calculations"

Annex A

The Finite Element Method

Introduction

Silvester and Ferrari [B2] and Jin [B3] offer a detailed explanation of how the Finite Element Method is derived from Maxwell's equations.

Excitations can be implemented through ports, which excite modes on transmission lines. This can be done in such a way that an S (scattering) matrix is produced automatically after solving the matrix equation. This is called the Transfinite Element Method and is discussed by Cendes and Lee in [B4].

Other possible excitations include voltage sources and incident waves. Incident waves are not limited to plane waves, but can also be spherical waves, cylindrical waves, Gaussian beams, and radiated fields produced by a simulation of an antenna in a different location in a separate model.

The mesh

In the Finite-Element Method, the computational domain is divided into many small volumes, the mesh elements, within which the field is approximated by simple basis functions with initially unknown coefficients. Mesh elements can have multiple shapes, such as bricks, prisms, tetrahedra and general hexahedra.

Brick-shaped elements in FEM have their use in simple geometries only. In the Finite-Difference Time-Domain Method one can make brick-shaped cells small and numerous enough to approximate a complicated geometry well. Also, techniques exist to compensate for "staircase" approximations of surfaces. In FEM, though, that isn't the case. Brick-shaped elements in FEM are not appropriate to model real-life wireless devices, their antennas, and human bodies.

Prism-shaped elements in FEM can be useful in layered geometries, such as printed circuit boards. They are not appropriate, though, to model real-life wireless devices, their antennas, and human bodies.

A tetrahedral mesh has the flexibility to combine small elements where needed with larger elements elsewhere is able to conform to any geometry while keeping the total mesh size, and thereby memory and CPU requirements, acceptable.

General hexahedra can be viewed as deformed bricks, with faces tilted and adjusted in size to conform to geometries in the model. Such elements, especially in an unstructured mesh, also have the necessary flexibility.

Therefore, this standard requires that the Finite Element Method used for SAR calculations employ a tetrahedral mesh or a general hexahedral mesh that has the flexibility to contain small and large elements simultaneously and to conform to the complicated geometries typically found in wireless devices, their antennas, their environment, and human bodies. This standard rejects meshes that are limited to brick-shaped or prism-shaped elements.

In regions in the computational domain that have little geometric detail and no large field gradients, the largest possible mesh element size in the Finite-Element method that still provides accurate solutions depends on the choice of the basis functions. If the basis functions are linear, mesh elements need to be smaller than a tenth of the local wavelength in the material. If the basis functions are quadratic, this increases to a third of a wavelength. The loss of accuracy with increasing element size is gradual.

Materials

In the Finite Element Method, material parameters are defined inside each object. In this method, there is no question which material takes priority on an interface between two objects: fields are computed unambiguously inside mesh elements and satisfy boundary conditions on interfaces between objects.

For electromagnetic simulations of SAR, usually the following material parameters are of interest: relative dielectric permittivity ϵ_r , bulk electric conductivity σ and mass density ρ . In almost all cases the relative magnetic permeability μ_r equals one.

The permittivity and conductivity tend to be frequency dependent. Since the material parameters don't exhibit rapid changes in bands encompassing individual antenna resonances, the frequency dependencies can be represented conveniently by data tables. Some software products will have built-in functions to describe frequency dependencies, such as the Debye model, the Lorentz model or the Cole-Cole model. Frequency-dependent material parameters ensure that the correct materials are used at every frequency. They have a consequence for the use of frequency sweeps, though. In frequency-domain methods, sophisticated frequency sweeps based on pole-zero expansions such as AWE or ALPS [B5,B6] may not be able to take frequency-dependent materials into account, and a choice needs to be made:

- Perform the frequency sweep by solving explicitly at multiple frequencies and interpolate;
- Use a pole-zero expansion for the frequency sweep but assume constant material parameters.

In this application, both are expected to give valid results, provided the material parameters chosen in the second case belong to a frequency point in the antenna resonance curve of interest, and the sweep range does not cover a second antenna resonance.

Boundary Conditions

In SAR simulations, two kinds of boundary conditions tend to be important: boundaries representing conducting metal surfaces and absorbing boundaries.

For any metal, the skin depth at the frequencies of interest will be small relative to other dimensions in the model. For instance, the skin depth of copper at 1 GHz is about 0.002 mm. In a printed-circuit board, copper is used and the thickness of traces and planes is usually at least 0.017 mm and more often 0.035 mm, i.e. many times the skin depth at 1 GHz. To solve inside metals explicitly, mesh elements in the metal would need to be as short as a fraction of a skin depth perpendicular to the surface and would have extreme aspect ratios. For accuracy, many mesh elements would be needed. Therefore, it is very inefficient to try to solve for fields inside the metals explicitly. Instead, metals should be handled through boundary conditions.

The surfaces of the metals should be assigned finite-conductivity boundary conditions. Alternatively, a PEC boundary condition can be used, which simply enforces zero tangential electric field. In practice, for this application, these two boundary conditions give almost the same results, since metal losses in a communication device are very small compared to other losses and have negligible effect on the fields. If there is any effect, the simulation with PEC will tend to radiate more power and show increased SAR relative to a simulation with finite conductivity boundaries, so there can be no incorrect certification due to the use of PEC boundaries.

Metals in a PCB as well as patch antennas can have aspect ratios of more than a thousand, e.g. be tens of mm long while being only a few hundredths of a mm thick. Mesh elements outside the metal, connecting to the sides of such objects, would also have very large aspect ratios. For accuracy, many mesh elements would be needed. In such a case, it is acceptable to model the metal as a 2D sheet rather than as a 3D object. This is expected to have negligible effect on the fields for this application.

In the Finite Element Method, the outer boundary of the computational domain needs to be terminated with a boundary condition. For SAR simulations, an absorption mechanism is needed that simulates radiation towards infinity, like the walls of an anechoic chamber do in measurements. Most often, a second-order absorbing boundary condition is used for this [B6]. Such a boundary condition has to be placed at least a quarter-wavelength away (more is better) from any objects and be convex. It is most effective when outgoing waves strike it perpendicularly and is not effective for grazing fields. Second-order radiation boundaries are accurate enough for the determination of SAR from wireless communication devices, provided the boundaries are convex and are placed more than a quarter wavelength away from any objects. More accuracy

can be obtained with higher-order radiation boundaries, with Perfectly Matched Layers (PMLs), and with a hybrid FEM-Boundary-Element Method. PMLs are layers of anisotropic absorbing material, first introduced by Berenger [B8, B9]. A recent improvement on them for Finite Elements is the concept of adaptive PMLs [B10], where one layer is sufficient and the mesh is refined adaptively inside. In the hybrid FEM-BEM method, the Finite Element Method is applied to a volume that includes all the objects, while the Method of Moments is applied on the surface of that encompassing volume in order to take care of the radiation [B11-B14]. This eliminates the need for absorbing boundaries or perfectly matched layers in the finite-element method. The matrix for this kind of approach has a sparse part for the FEM volume and a dense block for the surface of that volume.

Both with radiation boundaries and PMLs, the radiated fields outside the computational domain can be computed by integration over a closed surface inside the domain, e.g. the outer surface of the air volume surrounding all objects.

For calculations of power and efficiency, see IEC 62704-1, Annex A.6. That section contains a general description which does not depend on a particular choice of simulation method.

RF Source

An antenna in a numerical model can be fed in several ways. One can attach a wave port to a transmission line in order to excite it with an accurate representation of the propagating mode, or one can excite a feed point in a simpler way with the appropriate electric field or voltage between its terminals. In any case, part of the original CAD model has to be removed to give space for the excitation.

For a source model that includes lumped circuit elements the values for the elements are obtained from results of circuit simulation of the final stage of the RF amplifier or design data for the wireless device. These lumped elements, if included in the model, should be placed close to the RF source but still be a separate entity in the model.